Transaction B: Mechanical Engineering
Vol. 16, No. 5, pp. 440–450

SCIENTIA IRANICA

Determining Maximum Load Carrying Capacity of Flexible Link Manipulators

M.H. Korayem[1,*], R. Haghighi[1], A. Nikoobin[1], A. Alamdari[1] and A.H. Korayem[1]

Abstract. *In this paper, an algorithm is proposed to improve the Maximum Load Carrying Capacity (MLCC) of flexible robot manipulators. The maximum allowable load which can be achieved by a flexible manipulator along a given trajectory is limited by the joints' actuator capacity and the end effector accuracy constraint. In an open-loop approach, the end effector deviation from the predefined path is significant and the accuracy constraint restrains the maximum payload before actuators go into saturation mode. By using a controller, the accuracy of tracking will improve. The actuator constraint is not a major concern and, therefore, the full power of the actuators, which leads to an increase in the Maximum Load Carrying Capacity, can be used. In this case, the controller can play an important role in improving the maximum payload, so a robust controller is designed. However, the control strategy requires measurement of the elastic variables' velocity, which is not conveniently measurable. So, a nonlinear observer is designed to estimate these variables. A stability analysis of the proposed controller and state observer is performed on the basis of the Lyapunov Direct Method. In order to verify the effectiveness of the presented method, simulation is done for a two link flexible manipulator. The obtained maximum payload for open and closed-loop cases is compared, and the superiority of the method is illustrated.*

Keywords: *Maximum Load; Boundary layer sliding mode; Nonlinear state observer.*

INTRODUCTION

Finding the full load motion for a given point-to-point task can maximize the productivity and economic usage of the manipulators. The maximum allowable load of a fixed base manipulator is often defined as the maximum value of the load that a robot manipulator is able to carry on a desired trajectory which is based on a consideration of inertia effects on this desired path [1]. For rigid manipulators, the maximum load on a given trajectory is primarily constrained by the joint actuator torque and its velocity characteristic. However, for flexible manipulators another constraint, i.e. maximum allowable deflection, must be considered.

The maximum load carrying capacity along the given path can be determined in both open loop and closed-loop cases. In most previous works dealing with determining the DLCC along a given path, only dynamic equations have been used without considering the controller, while most manipulators in industrial applications are working based on feedback. In open loop cases, several algorithms are proposed for finding the maximum load carrying capacity of parallel robots [2], rigid mobile manipulators [3], flexible joint manipulators [4], flexible link manipulators [5], cable-suspended parallel manipulators [6] and redundant manipulators [7]. In the closed-loop case, the controller type and its parameters have a significant effect on increasing the maximum payload. In [8], a closed-loop approach has been employed to determine the DLCC of a flexible joint manipulator by considering a feedback linearization controller to track a predefined path. Another work, based on a sliding mode technique, has been undertaken for flexible joint manipulators in [9].

In flexible link manipulators, strong coupling between the nonlinear rigid-body motions and the linear elastic displacements of the links as well as the strong coupling between the elastic displacements of the links during large motions of the manipulator, makes the dynamics of flexible manipulators as highly coupled nonlinear time-varying MIMO systems with distributed parameters [10]. Complexities, such as

1. *Robotic Research Laboratory, Department of Mechanical Engineering, Iran University of Science and Technology, Tehran, P.O. Box 18846, Iran.*
*. *Corresponding author. E-mail: hkorayem@iust.ac.ir.*

Received 26 June 2008; received in revised form 6 February 2009; accepted 16 March 2009

the non-minimum-phase property of the tip transfer function that contains unstable zeros and complex poles in this transfer function and the existence of unstructured uncertainties due to the truncation of high-order resonance modes and system nonlinearities makes it difficult to accurately position the tip of the flexible manipulator [11-16]. Moreover, it creates a very challenging task in designing controllers for flexible manipulators. One method that is excessively used in the control of nonlinear systems is feedback linearization [17-19]. However, for flexible link robots, due to highly nonlinear coupled dynamics and the existence of passive degrees-of-freedom, only Partial Feedback Linearization (PFL) is suitable. For flexible link robots, the portion of the dynamics corresponding to the active degrees of freedom can be linearized by the nonlinear feedback. The remaining portion of the dynamics after such partial feedback linearization is nonlinear and represents internal dynamics [20]. A major drawback in this method, which cannot be used solely as a controller, is its lack of robustness with respect to uncertainties.

Sliding Mode Control (SMC), as a powerful method of tackling uncertain nonlinear systems, is particularly suited for complex systems such as flexible manipulators [21]. In the design of SMC, it is assumed that the control can be switched from one structure to another infinitely fast. However, because of the switching delay computation and the limitation of physical actuators that cannot handle the switching of the control signal at an infinite rate, it is practically impossible to achieve high-speed switching control. As a result of this imperfect control switching between structures, the system trajectory appears to chatter instead of sliding along the switching surface. Chatter involves high frequency control switching and may lead to the excitation of previously neglected high frequency system dynamics. Smoothing techniques, such as boundary layer normalization and replacement of the discontinuous control term by a fuzzy system [22,23] have been employed. The smoothing of control discontinuity inside the boundary layer essentially assigns a lowpass filter structure to the local dynamics of the variable, s, thus eliminating chatter.

An accurate knowledge of arm state variables is required by many advanced control techniques for flexible multi-link robots [24-29]. It can be conveniently achieved by using a state observer. Some works have been done using linear observers derived for a linearized model of the arm [30]. Other papers propose the use of nonlinear state observers to obtain the values of unmeasurable state variables [31-32]. In flexible manipulators, it is possible to measure joint positions, velocities and flexible modes of manipulators using shaft encoders, tachometers and strain gauges, respectively. However, measuring the flexural generalized velocities cannot be easily or accurately accomplished. Thus, a state observer is desirable in these circumstances. In order to decrease computational effort, a reduced order observer for estimating only flexible variables can be very helpful. The observer is designed based on a sliding mode approach. Similar to sliding mode controllers, sliding mode observers are designed by using sliding surfaces and offer robustness against both parametric uncertainties and external disturbances. The proposed observer requires positions and velocities of joints as well as flexible modes, and it estimates the rates of change of flexible modes.

An industrial manipulator usually requires six Degrees Of Freedom (DOF) in order to efficiently drive the gripper to a specified position with a prescribed orientation in the workspace. If it is constructed as a lightweight manipulator, practically, only the two-DOF rotary long links will be deformed under heavy loading and fast motion. So, the simulation is done for a two link flexible manipulator. In order to show the effectiveness of the proposed closed-loop algorithm, the simulation is done for both open loop and closed-loop cases. In closed-loop cases, the controller and the observer have been designed based on the first elastic mode of the beam, while the dynamic model is based on two elastic modes of the beam. The second elastic mode has been included to investigate the effects of unstructured uncertainties on the overall performance of the closed-loop system.

The paper is organized as follows: First, the general dynamic equations of a flexible link manipulator are derived. Then, by using partial feedback linearization, a controller is designed for a partially linearized model of a flexible manipulator based on a sliding mode approach. Following that, an algorithm is proposed to compute maximum allowable load by considering the limiting factors. Finally, some numerical result is shown.

DYNAMICS OF FLEXIBLE-LINK MANIPULATOR

Assuming that each arm does not undergo torsional deformations and considering an Euler-Bernoulli beam for each link, flexible-link robotic manipulators can be described as infinite-dimensional dynamical systems by using partial differential equations [33] (see Figure 1). In order to derive a finite-dimensional ordinary differential equation, an approximation approach using assumed mode methods, is taken into account.

By applying the Lagrange formulation, the dynamics of any multi-link flexible-link robot can be represented by:

$$M(q)\ddot{q} + N(q, \dot{q}) = \tau, \tag{1}$$

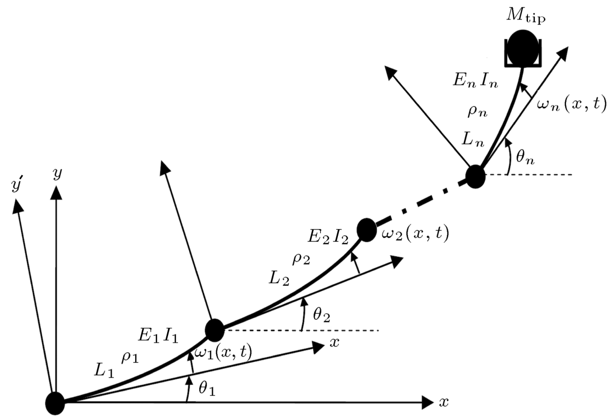

Figure 1. Flexible manipulator.

where $q(t)=[q_r^T,q_f^T]^T$, in which q_r is the vector of rigid modes (generalized joint coordinates) and q_f is the vector of flexible modes. $M(q)$ represents the inertia matrix, $N(q,\dot{q})$ is a $n\times 1$ vector of centripetal and Coriolis velocity terms.

The flexible manipulator dynamics are partitioned into rigid and flexible degrees-of-freedom as:

$$\begin{cases} M_{rr}\ddot{q}_r + M_{rf}\ddot{q}_f + N_r = u & \text{I} \\ M_{fr}\ddot{q}_r + M_{ff}\ddot{q}_f + N_f = 0 & \text{II} \end{cases} \tag{2}$$

where the following properties are known to be verified by the Lagrangian structure definite matrices.

Properties

I. $M(q), M_{rr}(q)$ and $M_{ff}(q)$ are non-singular, symmetric, positive definite matrices.

II. $M_{rr}+M_{rf}M_{ff}^{-1}M_{fr}$ is a symmetric positive-definite matrix.

CONTROLLER DESIGN

The controller design of a flexible link manipulator is divided into two steps. First, by applying partial feedback linearization, the dynamic of the flexible link is divided into two parts: a partially linearized model and an internal model. Second, use of the sliding mode approach forces the state trajectory of a system to the origin in the error phase hyperplane during two distinct phases: reaching phase and sliding phase.

Partial Feedback Linearization

For flexible manipulators that have a passive degree, instead of applying fully feedback linearization, it is convenient to use partial feedback linearization. The formulation of partial feedback linearization is as follows.

From Equation 2-II, $\ddot{q}_f$ can be expressed as below:

$$\ddot{q}_f = M_{ff}^{-1}[M_{fr}\ddot{q}_r - N_f]. \tag{3}$$

Substituting for $\ddot{q}_f$ from Equation 3 in Equation 2-I gives:

$$[M_{rr}+M_{rf}M_{ff}^{-1}M_{fr}]\ddot{q}_r + N_r - M_{rf}M_{ff}^{-1}N_f = u. \tag{4}$$

It can be easily seen that Equation 4 is similar in form to rigid manipulator modeling with the equivalent symmetric and positive definite mass matrix, $M_{rr} + M_{rf}M_{ff}^{-1}M_{fr}$, based on property II. The zero dynamic is defined for a nonlinear system Equation 2 by putting q_r and its derivatives equal to zero. So:

$$M_{ff}\ddot{q}_f + N_f = 0, \tag{5}$$

where N_f is simplified to Kq_f where:

$$K = \operatorname{diag}\{\omega_{11}^2, \omega_{12}^2, \ldots, \omega_{ij}^2, \cdots, \omega_{nm}^2\}. \tag{6}$$

So, Equation 5 can be written as:

$$M_{ff}\ddot{q}_f + Kq_f = 0. \tag{7}$$

Since M_{ff} and K are the positive definite symmetric matrices, the equilibrium point $[q_f,\dot{q}_f]$ of Equation 7 is stable in the sense of Lyapunov but not asymptotically stable.

Sliding Mode Design

In the sliding-mode control theory, control dynamics have two sequential modes; the first is the reaching mode and the second is the sliding mode. In particular, the Lyapunov sliding condition forces system states to reach a hyperplane and keeps them sliding on this hyperplane. Essentially, a SMC design is composed of two phases: hyperplane design and controller design. There are various methods for designing hyperplane [34], however, in this paper, a method proposed by Slotine is used [35]. In this method, the sliding surface is defined as:

$$s = (\dot{\tilde{q}}_r + \lambda'\dot{\tilde{q}}_f) + \lambda(\tilde{q}_r + \lambda'\tilde{q}_f), \tag{8}$$

where $\tilde{q}_r = q_r - q_r^{ref}$ and $\tilde{q}_f = q_f - q_f^{ref}$. q_r^{ref} is the desired trajectory of joints and $q_f^{ref} = 0$ because the desired value for flexible variables is zero. Also, λ and λ' are positive constants.

To determine the control law, the derivative of the sliding surface must be determined.

$$\dot{s} = (\ddot{\tilde{q}}_r + \lambda'\ddot{\tilde{q}}_f) + \lambda(\dot{\tilde{q}}_r + \lambda'\dot{\tilde{q}}_f). \tag{9}$$

Treating the term $\lambda'\ddot{\tilde{q}}_f$ as disturbance, Equation 9 is rearranged as below:

$$\dot{s} = \ddot{q}_r - \ddot{q}_r^{ref} + \lambda(\dot{\tilde{q}}_r + \lambda'\dot{\tilde{q}}_f). \tag{10}$$

Since the sliding condition is defined by:

$$\dot{s} \leq -K \text{ sign}(s), \tag{11}$$

so, Equation 10 in order to satisfy the sliding condition must be written as:

$$\ddot{q}_r - \ddot{q}_r^{ref} + \lambda(\dot{\tilde{q}}_r + \lambda' \dot{\tilde{q}}_f) = -K \text{ sign}(s). \tag{12}$$

By substituting $\ddot{q}_r$ from Equation 4, Equation 12 becomes:

$$[M_{rr} + M_{rf} M_{ff}^{-1} M_{fr}]^{-1} [u - N_r - M_{rf} M_{ff}^{-1} N_f]$$
$$- (\ddot{q}_r^{ref} - \lambda(\dot{\tilde{q}}_r + \lambda' \dot{\tilde{q}}_f) = -K \text{ sign}(s). \tag{13}$$

By extracting u from Equation 13, the control law is defined as:

$$u = M[\ddot{q}_r^{ref} - \lambda(\dot{\tilde{q}}_r + \lambda' \dot{\tilde{q}}_f) - K \text{ sign}(s)] + N, \tag{14}$$

where $M = [M_{rr} + M_{rf} M_{ff}^{-1} M_{fr}]$ and $N = N_r - M_{rf} M_{ff}^{-1} N_f$. From the practical point of view, deriving the exact model of the system is a hard task, so it is convenient to use the nominal model. By defining the $\hat{M}$ and $\hat{N}$ which are the nominal values of M and N, respectively, the control law can be rewritten as follows:

$$u = \hat{M}[\ddot{q}_r^{ref} - \lambda(\dot{\tilde{q}}_r + \lambda' \dot{\tilde{q}}_f) - K \text{ sign}(s)] + \hat{N}. \tag{15}$$

Stability Analysis of SMC

For purpose of design integrity, a simple stability analysis based on the Lyapunov Direct method is carried out. The Lyapunov function candidate is defined as follows:

$$V = \frac{1}{2} s^2. \tag{16}$$

Differentiating Equation 16 and using Equations 4, 11 and 15, one can write:

$$\dot{V} = s\dot{s} = s\{M^{-1}[\hat{M}[\ddot{q}_r^{ref} - \lambda(\dot{\tilde{q}}_r + \lambda' \dot{\tilde{q}}_f)$$
$$-K \text{ sign}(s)] + \hat{N} - N] - \ddot{q}_r^{ref} - \lambda(\dot{\tilde{q}}_r + \lambda' \dot{\tilde{q}}_f)\}. \tag{17}$$

By using simplification, Equation 17 becomes:

$$\dot{V} = s\{M^{-1}\hat{M}[\ddot{q}_r^{ref} - \lambda(\dot{\tilde{q}}_r + \lambda' \dot{\tilde{q}}_f) - K \text{ sign}(s)]$$
$$+ M^{-1}\Delta N - \ddot{q}_r^{ref} - \lambda(\dot{\tilde{q}}_r + \lambda' \dot{\tilde{q}}_f)\}. \tag{18}$$

For stability $\dot{V}$ must be negative. Since $\dot{V} = s\dot{s}$ another condition that assures the stability of the system can be defined as $s\dot{s} \leq -\eta|s|$ or $\dot{s} \leq -\eta \text{ sign}(s)$ which is called a sliding condition. By applying the sliding condition, we have:

$$(M^{-1}\hat{M} - I)(\ddot{q}_r^{ref} - \lambda(\dot{\tilde{q}}_r + \lambda' \dot{\tilde{q}}_f))$$
$$- M^{-1}\hat{M}.K.\text{sign}(s) + M^{-1}\Delta N \leq -\eta.\text{sign}(s). \tag{19}$$

By multiplication of both sides of Equation 19 by $\hat{M}^{-1}M$, one gets:

$$(I - \hat{M}^{-1}M)(\ddot{q}_r^{ref} - \lambda(\dot{\tilde{q}}_r + \lambda' \dot{\tilde{q}}_f))$$
$$- K.\text{sign}(s) + \hat{M}^{-1}\Delta N \leq -\hat{M}^{-1}M\eta.\text{sign}(s). \tag{20}$$

So, the condition which guarantees the stability can be expressed as follows:

$$K > |(I - \hat{M}^{-1}M)(\ddot{q}_r^{ref} - \lambda(\dot{\tilde{q}}_r + \lambda' \dot{\tilde{q}}_f))$$
$$+ \hat{M}^{-1}\Delta N| + \hat{M}^{-1}M\eta. \tag{21}$$

Since M is unknown, one can define the following known bounds:

$$M_{\min} \leq M \leq M_{\max}. \tag{22}$$

Since M acts multiplicatively in the dynamics of the manipulator, it is reasonable to choose the estimate $\hat{M}$ of M as the geometric means of the above bounds [35]:

$$\hat{M} = (M_{\min} M_{\max})^{1/2}. \tag{23}$$

Therefore, the bounds for $\hat{M}^{-1}M$ can be defined as follows:

$$\Psi^{-1} \leq \hat{M}^{-1}M \leq \Psi, \tag{24}$$

where:

$$\Psi = \left(\frac{M_{\max}}{M_{\min}}\right)^{1/2}. \tag{25}$$

So, Equation 21 can be rewritten in terms of Ψ:

$$K > |(I - \Psi)(\ddot{q}_r^{ref} - \lambda(\dot{\tilde{q}}_r + \lambda' \dot{\tilde{q}}_f)) + \hat{M}^{-1}\Delta N| + \Psi\eta. \tag{26}$$

Boundary Layer

An essential drawback of SMC is that owing to the signum term, it causes abrupt changes (chattering) to the control signal, u. However, this can be avoided by introducing a boundary layer (Φ) from both sides of the sliding surface, $s = 0$, as shown in Figure 2.

By applying a boundary layer at both sides of the sliding surface, Equation 15 is written as below:

$$u = \hat{M}\left[\ddot{q}_r^{ref} - \lambda(\dot{\tilde{q}}_r + \lambda' \dot{\tilde{q}}_f) - K \text{ sat}\left(\frac{s}{\Phi}\right)\right] + \hat{N}, \tag{27}$$

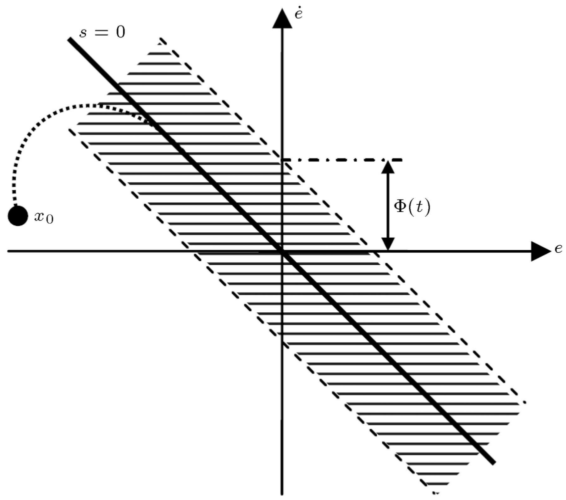

Figure 2. Variable boundary layer.

where "sat" is saturation function. If we rewrite $\dot{s}$ based on the "sat" function, we have:

$$\dot{s} =(M^{-1}\hat{M} - I)(\ddot{q}_r^{ref} - \lambda(\dot{\tilde{q}}_r + \lambda'\dot{\tilde{q}}_f)) - M^{-1}\hat{M}.K.\text{sat}\left(\frac{s}{\Phi}\right) + M^{-1}\Delta N. \tag{28}$$

By considering the system trajectories inside the boundary layer:

$$\dot{s} =(M^{-1}\hat{M} - I)(\ddot{q}_r^{ref} - \lambda(\dot{\tilde{q}}_r + \lambda'\dot{\tilde{q}}_f)) - M^{-1}\hat{M}.K.\left(\frac{s}{\Phi}\right) + M^{-1}\Delta N, \tag{29}$$

and Equation 29 can be rewritten as:

$$\dot{s}+\frac{M^{-1}\hat{M}.K}{\Phi}s = (M^{-1}\hat{M} - I) (\ddot{q}_r^{ref} - \lambda(\dot{\tilde{q}}_r + \lambda'\dot{\tilde{q}}_f)) + M^{-1}\Delta N. \tag{30}$$

In fact, Equation 30 shows that the smoothing of control discontinuity inside the boundary layer essentially assigns a low pass filter structure to the local dynamics of the variable, s, thus, eliminating chattering. Furthermore, the sliding condition is redefined as below:

$$\dot{s} \leq (\dot{\Phi} - K)\text{sign}(s). \tag{31}$$

In the presence of a boundary layer, we need to guarantee that the distance from the boundary layer always decreases. System robustness is a function of the boundary layer; in other words, a thinner boundary layer gives more robust control, but larger chattering.

STATE OBSERVER DESIGN

In the control law (Equation 15), measurements of the velocity of elastic variables are needed and since it cannot easily be measured, there is a demand to design a state observer for the measuring of these variables. By extracting $\ddot{q}_r$ from Equation 2-I, and substituting in Equation 2-II, we have:

$$M_{fr}M_{rr}^{-1}[u - M_{rf}\ddot{q}_f - N_r] + M_{ff}\ddot{q}_f + N_f = 0, \tag{32}$$

and it can be rearranged to:

$$[M_{ff} - M_{fr}M_{rr}^{-1}M_{rf}]\ddot{q}_f + N_f - M_{fr}M_{rr}^{-1}N_r + M_{fr}M_{rr}^{-1}u = 0. \tag{33}$$

Equation 33 can be expressed in state space form:

$$\begin{cases} \dot{x}_{f_1} = x_{f_2} \\ \dot{x}_{f_2} =[M_{ff} - M_{fr}M_{rr}^{-1}M_{rf}]^{-1} \\ \qquad [-N_f + M_{fr}M_{rr}^{-1}N_r - M_{fr}M_{rr}^{-1}u] \end{cases} \tag{34}$$

where $x_{f_1} = q_f$ and $x_{f_2} = \dot{q}_f$.

Using a sliding mode observer technique, the dynamic of the observer is written as:

$$\begin{cases} \dot{\hat{x}}_{f_1} = \hat{x}_{f_2} + k_{11}\tilde{x}_{f_1} + k_{12}\text{sign}(\tilde{x}_{f_1}) \\ \dot{\hat{x}}_{f_2} = \hat{f}(x_r, x_{f_1}, \hat{x}_{f_2}) + k_{21}\tilde{x}_{f_1} + k_{22}\text{sign}(\tilde{x}_{f_1}) \end{cases} \tag{35}$$

where $\hat{f}(x_r, x_{f_1}, \hat{x}_{f_2}) = [M_{ff} - M_{fr}M_{rr}^{-1}M_{rf}]^{-1}[-N_f + M_{fr}M_{rr}^{-1}N_r - M_{fr}M_{rr}^{-1}u]$ and k_{ij} are positive parameters. $\tilde{x}_{f_1}$ is the estimation error and equal to $x_{f_1} - \hat{x}_{f_1}$.

The dynamic of error is achieved by subtracting Equation 34 from Equation 35:

$$\begin{cases} \dot{\tilde{x}}_{f_1} = \tilde{x}_{f_2} - k_{11}\tilde{x}_{f_1} - k_{12}\text{sign}(\tilde{x}_{f_1}) \\ \dot{\tilde{x}}_{f_2} = \tilde{f} - k_{21}\tilde{x}_{f_1} - k_{22}\text{sign}(\tilde{x}_{f_1}) \end{cases} \tag{36}$$

where it can be written in the following simple form:

$$\dot{e} = \tilde{f}^* - K_e e - K_s\text{sign}(e), \tag{37}$$

where $\tilde{f}^* = \begin{bmatrix} \tilde{x}_{f_2} \\ \tilde{f} \end{bmatrix}$ and $e = \begin{bmatrix} \tilde{x}_{f_1} \\ \tilde{x}_{f_2} \end{bmatrix}$. Using Taylor expansion around $e = 0$, Equation 37 can be given as:

$$\dot{e} = Ae + O(e^2) - K_s \text{ sign}(e), \tag{38}$$

where:

$$A = \left(\frac{\partial \tilde{f}^*}{\partial e} - K_e\right)_{e=0} = \begin{bmatrix} 0 & 1 \\ \frac{\partial \tilde{f}}{\partial \tilde{x}_{f_1}}\Big|_{\tilde{x}_{f_1}=0} & \frac{\partial \tilde{f}}{\partial \tilde{x}_{f_2}}\Big|_{\tilde{x}_{f_2}=0} \end{bmatrix} + \begin{bmatrix} -k_{11} & 0 \\ -k_{21} & 0 \end{bmatrix}. \tag{39}$$

The eigenvalues of A can be specifically placed by properly choosing K_e. If matrix A has negative eigenvalues (it must be a negative definite matrix), then the error will converge to zero.

From matrix algebra, we know that a square matrix is negative definite if determinants of all principal minors have the following pattern:

$$|D_1| < 0, \ |D_2| > 0, \ |D_3| < 0, \cdots , \tag{40}$$

where D_i is the ith principle minor. So, by applying the above conditions, we have:

$$-k_{11}\frac{\partial \tilde{f}}{\partial \tilde{x}_{f_2}}\bigg|_{\tilde{x}_{f_2}=0} + k_{21} - \frac{\partial \tilde{f}}{\partial \tilde{x}_{f_1}}\bigg|_{\tilde{x}_{f_1}=0} > 0. \tag{41}$$

It can be easily seen that, if k_{21} is chosen big enough, the above condition is satisfied.

DETERMINING MAXIMUM LOAD CARRYING CAPACITY

The maximum allowable load of a fixed base manipulator is often defined as the maximum payload that can be carried by the manipulator with acceptable accuracy. For rigid manipulators, it can be seen that MLCC is directly in relation to actuator strength, while for flexible manipulators additional constraints must be considered and that is maximum allowable deflection which depends on flexible variables.

The above condition can be taken into account in MLCC determination by imposing a constraint on the end effector deflection, in addition to the actuator torque constraint imposed for rigid manipulators. Deflection of the end effector can cause excessive deflection from the pre-defined trajectory, even though the joint torque constraints are not violated. By considering the actuator torque and deflection constraints and adopting a logical computing method, the maximum load-carrying capacity of a flexible manipulator for a pre-defined trajectory can be computed.

MLCC can be obtained in either open loop or closed-loop cases. In open loop, the controller is not considered, and only a dynamic equation is used. In closed-loop cases, MLCC is obtained, while both the dynamic equation and controller are considered. The actuator torque constraint is formulated on the basis of the typical torque-speed characteristics of DC motors:

$$\begin{cases} \tau_U = K_1 - K_2\dot{q} \\ \tau_L = -K_1 - K_2\dot{q} \end{cases} \tag{42}$$

where τ_U and τ_L are the upper bound and the lower bound of the actuator constraint, respectively. The coefficients K_i are defined as:

$$\begin{cases} K_1 = T_s \\ K_2 = \frac{T_s}{\omega_{nl}} \end{cases} \tag{43}$$

where T_s is the stall torque and ω_{nl} is the maximum no-load speed of the motor.

In the following sections, determining the MLCC is presented for these two cases.

Determining MLCC in Open Loop Case

For computing the maximum load carrying capacity in an open loop condition, the following steps must be taken:

1. Determining the actuator path within which the arms are in fully extended configurations;
2. Finding $q_r, \dot{q}_r, \ddot{q}_r$ by solving the inverse dynamic for the same rigid manipulator;
3. Determining $q_f, \dot{q}_f, \ddot{q}_f$ from Equation 2-II;
4. Computation of the actuators torque (τ_{nl}) and end effector path for a no load manipulator;
5. Choosing an initial value for m_{max};
6. Putting $m_p = m_{\max}$ and computing the actuators torque (τ_l) and end effector path;
7. Compute the actuators bounds based on Equations 42 and 43;
8. Determining the load coefficient C_a based on actuator constraints [8]:

$$C_a = \min(\min(C_a^{\text{first joint}}(1:n)), \quad \min(C_a^{\text{second joint}}(1:n))). \tag{44}$$

9. Determining the load coefficient C_p based on accuracy constraints:

$$C_p(k) = \frac{R_p - \Delta_e(k)}{\max(\Delta_e(k)) - \max(\Delta_n(k))}, \tag{45}$$

   where $\Delta_e(k)$ is the error of the end effector in the presence of load and $\Delta_n(k)$ is the error of the end effector without load.

10. Determining the load coefficient C

$$C = \min(C_p, C_a). \tag{46}$$

11. If $|C^{i+1} - C^i| \leq$ error then $m_{\max} = C \times m_p$, otherwise $m_p = C \times m_p$ and go to 6.

Determining MLCC in Closed-Loop Case

The algorithm used for finding MLCC in closed-loop cases, as shown in Figure 3. In closed-loop cases, the actuator constraint is the major parameter in determining MLCC, while in open loop cases the end effector accuracy is the major parameter in determining MLCC. The desired path is chosen the same as in open loop cases to compare these two cases. Since in

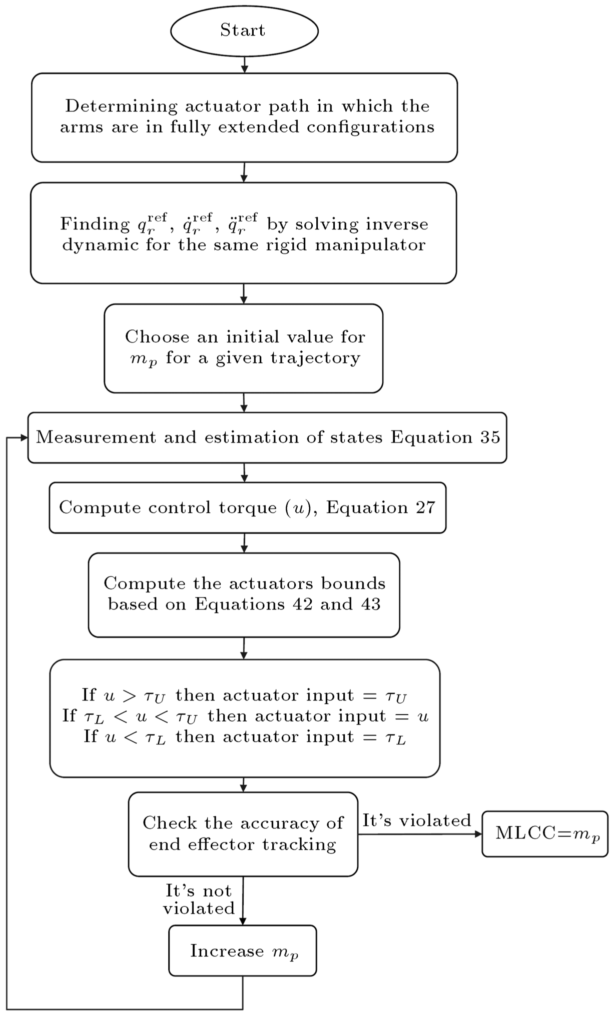

Figure 3. Flowchart of computing dynamic load carrying capacity.

closed-loop cases the system input is computed by a controller for applying the actuator constraints instead of defining the load coefficient, we put a constraint on the controller output such that, if controller output doesn't violate the actuator constraint, the system input is equal to controller output, otherwise, it is equal to the bounds of actuator constraints.

The accuracy constraint is checked by the distance between the desired and actual trajectory, which must not violate the accuracy constraint.

As can be seen, the controller plays a major role in determining the maximum load carrying capacity; in other words, improvement in controller leads to increasing MLCC.

SIMULATION STUDIES

To investigate the proposed algorithm, some simulation studies are presented for a two link flexible manipulator. In these studies, a specified trajectory for the load is assumed. Note that the second elastic mode is included in the model to investigate the effects of unstructured uncertainties on the overall performance of the closed-loop system. By applying the proposed algorithm for a closed-loop plant, the maximum allowable load was computed to be $m_{\text{load}} = 4.51$, meanwhile, the maximum allowable loop for an open loop in three iterations was found to be $m_{\text{load}} = 3.63$. The simulation results are shown in Figures 4 to 7. The parameters used in the simulation are given in Table 1.

Figure 4 shows the elastic variables in an open loop case, wherein these variables do not converge to zero. Figure 5 shows that in a closed loop case, the capacity of the actuators is better in comparison to the open loop case. Figure 6 shows the good performance of the state observer in estimating elastic variable velocities. Moreover, it shows the convergence of flexible link vibrations. Figure 7 shows the elastic variables used in the dynamic of the system, but in the controller and observer design, it is neglected to show the robustness of the controller, with respect to unstructured uncertainties.

Another simulation is done for a flexible robot manipulator with less rigidity. The parameters of the simulation are shown in Table 2. In this case, the

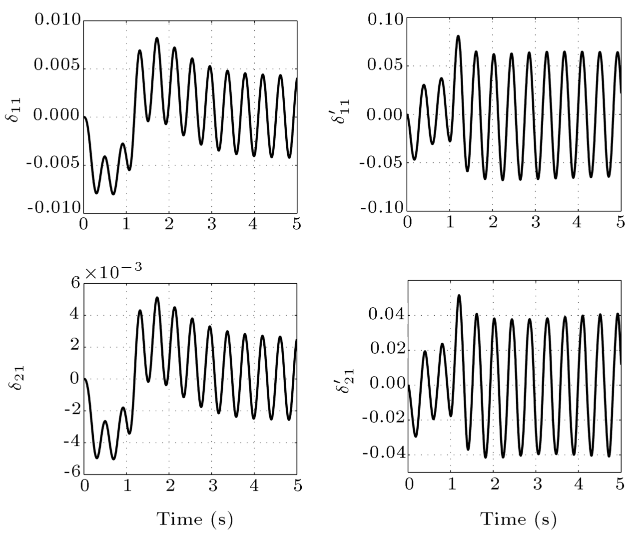

Figure 4. Flexible mode shapes in open loop case.

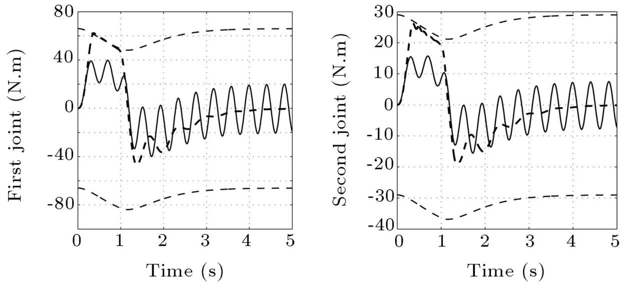

Figure 5. Control torque in two cases; open loop (solid thin line) and closed-loop (dashed thick line).

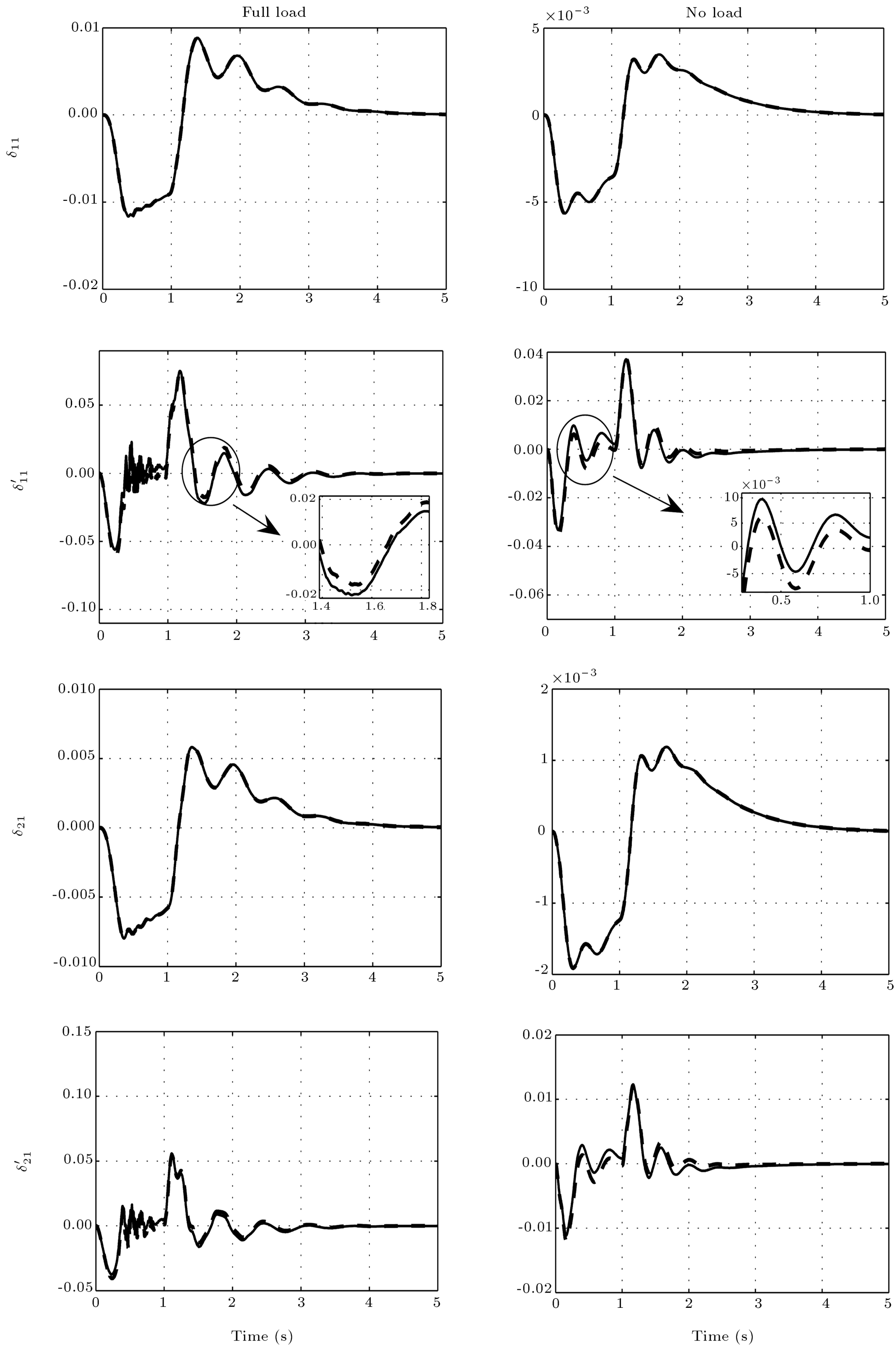

Figure 6. Flexible mode shapes in two cases (without load and full load); the actual signal is shown in solid thin line and the estimated variables are shown in dashed thick line (closed-loop case).

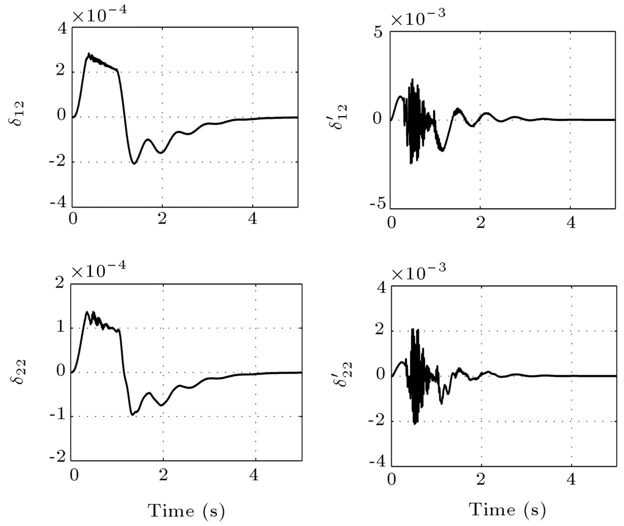

Figure 7. Flexible mode shapes considered only in plant (closed-loop case).

Table 1. Parameters of the simulation.

Parameter	Value	Unit
Length of links	$L_1 = L_2 = 1$	m
Density	$\rho_1 = \rho_2 = 4.68$	kg/m
Flexural rigidity	$E_1 I_1 = E_2 I_2 = 1025$	N.m^2
Actuator stall torque	$T_{s1} = 66,\ T_{s2} = 29$	N.m
Actuator no-load speed	$\omega_{n1} = \omega_{n2} = 3.5$	Rad/s
Controller constants	$\lambda = 10, K = 25$	
Observer constants	$k_{11} = 100,\ k_{12} = 1e5$ $k_{21} = 100,\ k_{22} = 1e5$	

Table 2. Parameters used for simulation.

Parameter	Value	Unit
Length of links	$L_1 = L_2 = 1$	m
Density	$\rho_1 = \rho_2 = 4.68$	kg/m
Flexural rigidity	$E_1 I_1 = E_2 I_2 = 100$	N.m^2
Actuator stall torque	$T_{s1} = 46, T_{s2} = 19$	N.m
Actuator no-load speed	$\omega_{n1} = \omega_{n2} = 3.5$	Rad/s

maximum load carrying capacity computed as $m_{\text{load}} = 2.74$ in open loop and as $m_{\text{load}} = 3.87$ in closed loop. The simulation result is shown in Figures 8 and 9.

CONCLUSION

The main objective of this investigation was to determine the maximum load for a flexible link manipulator in the presence of a controller. Therefore, in this case, except for actuator constraints, end effector accuracy should be considered. The controller is designed based on a sliding mode method, and for alleviation of the chattering phenomena a boundary layer is used. However, in a control law, the velocity of the elastic variables, which cannot be measured easily, is used. So, a nonlinear state observer is designed based on a sliding mode approach to estimate these variables. The controllers and the observer have been designed in this study, based on a simplified version of the model of the arm in which only the first elastic mode of the link is taken into account, while for the model, the second mode shape is also considered in order to investigate the effects of unstructured uncertainties on the overall performance of the closed-loop system. By applying the proposed algorithm for a closed-loop case, the maximum allowable load computed as $m_{\text{load}} = 4.51$, meanwhile, the maximum allowable loop for open loop was found as $m_{\text{load}} = 3.63$.

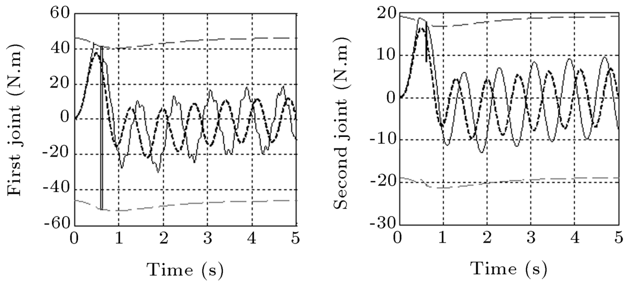

Figure 8. Control torque in two cases; closed-loop (solid thin line) and open loop (dashed thick line).

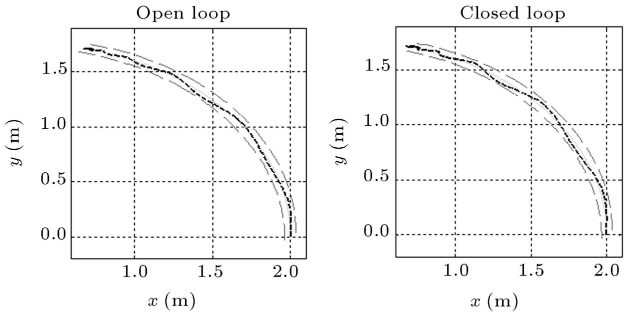

Figure 9. End effector path in two cases; open loop and closed-loop.

REFERENCES

1. Yao, Y.L., Korayem, M.H. and Basu, A. "Maximum allowable load of flexible manipulators for given dynamic trajectory", *Robotics and Computer-Integrated Manufacturing*, **10**(4), pp. 301-309 (1993).
2. Korayem, M.H. and Shokri, M. "Maximum dynamic load carrying capacity of a 6UPS-stewart platform manipulator", *Scientia Iranica*, **15**(1), pp. 131-143 (2008).

3. Korayem, M.H., Ghariblu, H. and Basu, A. "Maximum allowable load of mobile manipulators for two given end points of end effector", *International Journal of Advanced Manufacturing Technology*, **24**(9-10), pp. 743-751 (2004).
4. Korayem, M.H. and Nikoobin, A. "Maximum payload for flexible joint manipulators in point-to-point task using optimal control approach", *International Journal of Advanced Manufacturing Technology*, **38**(9-10), pp. 1045-1060 (2008).
5. Korayem, M.H., Heidari, A. and Nikoobin, A. "Maximum allowable dynamic load of flexible mobile manipulators using finite element approach", *International Journal of Advanced Manufacturing Technology*, **36**(5-6), pp. 606-617 (2008).
6. Korayem, M.H. and Bamdad, M. "Dynamic load-carrying capacity of cable-suspended parallel manipulators", *International Journal of Advanced Manufacturing Technology*, **44**(7-8), pp. 829-840 (2009).
7. Korayem, M.H. and Nikoobin, A. "Maximum payload path planning for redundant manipulator using indirect solution of optimal control problem", *International Journal of Advanced Manufacturing Technology*, **44**(7-8), pp. 725-736 (2009).
8. Korayem, M.H., Davarpanah, F. and Ghariblu, H. "Load carrying capacity of flexible joint manipulators with feedback linearization", *International Journal of Advanced Manufacturing Technology*, **29**(3-4), pp. 389-397 (2006).
9. Korayem, M.H. and Pilechian, A. "Maximum allowable load of elastic joint robots: Sliding mode control approach", *Amirkabir Journal of Science & Technology*, **17**(65), pp. 75-82 (2007).
10. Chen, W. "Dynamic modeling of multi-link flexible robotic manipulators", *Computers and Structures*, **79**(2), pp. 183-195 (2001).
11. Oke, G. and Istefanopulos, Y. "Tip position control of a two-link flexible robot manipulator based on nonlinear deflection feedback", *Chaos, Solitons and Fractals*, **17**(2), pp. 499-504 (2003).
12. Zhang, N., Feng, Y. and Yu, X. "Optimization of terminal sliding control for two-link flexible manipulators", *Proc. of IECON Industrial Electronic Conference*, **2**, pp. 1318-1322 (2004).
13. Ho, M.T. and Tu, Y.W. "Position control of a single-link flexible manipulator using H8-based PID control", *IEE Proc.: Control Theory and Applications*, **153**(5), pp. 615-622 (2006).
14. Halevi, Y. and Nachshoni, C.W. "Transfer function modeling of multi-link flexible structures", *Journal of Sound and Vibration*, **296**(1-2), pp. 73-90 (2006).
15. Maouche, A.R. and Attari, M. "Hybrid control strategy for flexible manipulators", *IEEE International Symposium on Industrial Electronics*, pp. 50-55 (2007).
16. Fan, T. and de Silva, C.W. "Dynamic modelling and model predictive control of flexible-link manipulators", *International Journal of Robotics and Automation*, **23**(4), pp. 227-234 (2008).
17. Yang, T.W., Xu, W.L., Tso, S.K. and Vincent, T.L. "Dynamic modeling based on real-time deflection measurement and compensation control for flexible multi-link manipulators", *Dynamics and Control*, **11**(1), pp. 5-24 (2001).
18. Benosman, M. and Le Vey, G. "Control of flexible manipulators: A survey", *Robotica*, **22**(5), pp. 533-545 (2004).
19. Kermani, M.R., Moallem, M. and Patel, R.V. "Study of system parameters and control design for a flexible manipulator using piezoelectric transducers", *Smart Materials and Structures*, **14**(4), pp. 843-849 (2005).
20. Arisoy, A., Gokasan, M. and Bogosyant, S. "Sliding mode based position control of a flexible-link arm", *12th International Conference on Power Electronics and Motion Control*, pp. 402-407 (2007).
21. Perruquetti, W. and Barbot, J.P. "Sliding mode control in engineering", *Marcel Deckker*, New York (2002).
22. Derbel, N. and Alimi, A.M. "Design of a sliding mode controller by fuzzy logic", *International Journal of Robotics and Automation*, **21**(4), pp. 241-246 (2006).
23. Thinh Ngo, H.Q., Shin, J.H. and Kim, W.H. "Fuzzy sliding mode control for a robot manipulator", *Artificial Life and Robotics*, **13**(1), pp. 124-128 (2008).
24. Li, Y.F. and Chen, X.B. "End-point sensing and state observation of a flexible-link robot", *IEEE/ASME Trans. on Mechatronics*, **6**(3), pp. 351-356 (2001).
25. Zaki, A., ElBeheiry, E.S. and ElMaraghy, W. "Variable structure observer design for flexible-link manipulator control", *Transactions of the Canadian Society for Mechanical Engineering*, **27**(1-2), pp. 107-129 (2003).
26. Parsa, K. "Dynamics, state estimation, and control of manipulators with rigid and flexible subsystems", PhD Dissertation, McGill University (2003).
27. Zuyev, A. and Sawodny, O. "Observer design for a flexible manipulator model with a payload", *Proc. of the IEEE Conference on Decision and Control*, pp. 4490-4495 (2006).
28. Caracciolo, R., Richiedei, D. and Trevisani, A. "Design and experimental validation of piecewise-linear state observers for flexible link mechanisms", *Meccanica*, **41**(6), pp. 623-637 (2006).
29. Tavasoli, A., Eghtesad, M. and Jafarian, H. "Two-time scale control and observer design for trajectory tracking of two cooperating robot manipulators moving a flexible beam", *Proc. of the American Control Conference*, **9-13**, pp. 735-740 (2007).
30. Zuyev, A.L. "Observability of a flexible manipulator with a payload", *Physics and Control*, **24-26**, pp. 523-526 (2005).
31. Nguyen, T.D. and Egeland, O. "Observer design for a flexible robot arm with a tip load", *American Control Conference*, **2**(8-10), pp. 1389-1394 (2005).
32. Chalhoub, N.G. and Kfoury, G.A. "Development of a robust nonlinear observer for a single-link flexible manipulator", *Nonlinear Dynamics*, **39**(3), pp. 217-233 (2005).

33. Lee, S.H. and Lee, C.W. "Hybrid control scheme for robust tracking of two-link flexible manipulator", *Journal of Intelligent and Robotic Systems*, **32**(4), pp. 389-410 (2001).

34. Nguyen, D.K. "Sliding mode control: Advanced design techniques", PhD Dissertation, University of Technology, Sydney, Australia (1998).

35. Slotine, J.J. and and Li, W. "Applied nonlinear control", *Prentice-Hall*, Englewood Cliffs, NJ (1991).